



HAL
open science

Close look on cubic Tm:KY 3 F 10 crystal for highly efficient lasing on the $3 H 4 \rightarrow 3 H 5$ transition

Lauren Guillemot, Pavel Loiko, Rémi Soulard, Alain Braud, Jean-Louis Doualan, Ammar Hideur, Patrice Camy

► To cite this version:

Lauren Guillemot, Pavel Loiko, Rémi Soulard, Alain Braud, Jean-Louis Doualan, et al.. Close look on cubic Tm:KY 3 F 10 crystal for highly efficient lasing on the $3 H 4 \rightarrow 3 H 5$ transition. Optics Express, 2020, 28 (3), pp.3451. 10.1364/OE.382650 . hal-02747031

HAL Id: hal-02747031

<https://hal.science/hal-02747031>

Submitted on 18 Dec 2023

HAL is a multi-disciplinary open access archive for the deposit and dissemination of scientific research documents, whether they are published or not. The documents may come from teaching and research institutions in France or abroad, or from public or private research centers.

L'archive ouverte pluridisciplinaire **HAL**, est destinée au dépôt et à la diffusion de documents scientifiques de niveau recherche, publiés ou non, émanant des établissements d'enseignement et de recherche français ou étrangers, des laboratoires publics ou privés.



Distributed under a Creative Commons Attribution 4.0 International License



Close look on cubic Tm:KY₃F₁₀ crystal for highly efficient lasing on the ³H₄ → ³H₅ transition

LAUREN GUILLEMOT,¹  PAVEL LOIKO,¹ RÉMI SOULARD,^{1,2} ALAIN BRAUD,¹ JEAN-LOUIS DOULAN,¹ AMMAR HIDEUR,³ AND PATRICE CAMY^{1,*}

¹Centre de recherche sur les Ions, les Matériaux et la Photonique (CIMAP), UMR 6252

CEA-CNRS-ENSICAEN, Université de Caen Normandie, 6 Boulevard du Maréchal Juin, 14050 Caen Cedex 4, France

²Laboratoire ARTEMIS, UMR 7250 Université Côte d'Azur-CNRS-Observatoire de la Côte d'Azur, F-06304 Nice, France

³CORIA UMR 6614, CNRS-INSA-Université de Rouen, Normandie Université, Avenue de l'université, BP. 12, 76801 Saint Etienne du Rouvray, France

*patrice.camy@ensicaen.fr

Abstract: We report on Czochralski growth, detailed ground- and excited-state absorption and emission spectroscopy and highly-efficient mid-infrared (~2.3 μm) laser operation of a cubic potassium yttrium fluoride crystal, Tm:KY₃F₁₀. The peak stimulated-emission cross-section for the ³H₄ → ³H₅ transition is 0.34×10⁻²⁰ cm² at 2345 nm with an emission bandwidth exceeding 50 nm. The excited-state absorption spectra for the ³F₄ → ³F_{2,3} and ³F₄ → ³H₄ transitions are measured and the cross-relaxation is quantified. A continuous-wave 5 at.% Tm:KY₃F₁₀ laser generated 0.84 W at 2331-2346 nm by pumping at 773 nm, with a record-high slope efficiency of 47.7% (versus the incident pump power) owing to the efficient action of energy-transfer upconversion leading to a pump quantum efficiency approaching 2. The first Tm:KY₃F₁₀ laser with ESA-assisted upconversion pumping (at 1048 nm) is also demonstrated. Due to its broadband emission properties, Tm:KY₃F₁₀ is promising for ultrashort pulse generation at ~2.3-2.4 μm.

© 2020 Optical Society of America under the terms of the [OSA Open Access Publishing Agreement](#)

1. Introduction

Ultrafast laser sources emitting in the “molecular fingerprint” near-mid-infrared spectral range of 2-3 μm are attractive for molecular spectroscopy, environmental sensing, medicine, multi-photon imaging and pumping of nonlinear frequency converters accessing emission wavelengths up to 20 μm [1,2]. In particular, the emission around 2.3 μm falls into the atmospheric transparency window and spectrally overlaps with absorption lines of carbon monoxide (CO), formaldehyde (H₂CO), methane (CH₄) and glucose (C₆H₁₂O₆) molecules [3,4]. A well-known approach to generate femtosecond (fs) pulses at such wavelengths is to employ Cr²⁺-doped II-VI chalcogenides (ZnS, ZnSe) in mode-locked lasers [5,6]. However, the fabrication of these crystals of good optical quality is complicated.

Recently, another type of mode-locked lasers delivering fs pulses at ~2.3 μm directly out of the oscillator was proposed based on thulium (Tm³⁺) ions [7,8]. Tm³⁺ (electronic configuration: [Xe]4f¹²) provides near-mid-infrared emission due to the ³H₄ → ³H₅ 4f-4f transition [9]. The main difficulty here is that the upper laser lifetime (³H₄) may be quenched due to different reasons such as multiphonon non-radiative (NR) relaxation, cross-relaxation (CR) among adjacent Tm³⁺ ions, ³H₄ + ³H₆ → ³F₄ + ³F₄, or energy-migration (EM) to defects and impurities. The rate of NR relaxation strongly depends on the maximum phonon energy of the host. Both CR and EM are dependent on the Tm³⁺ doping level. Thus, a proper material (and the doping level) should be found for efficient 2.3 μm laser operation. This goal has not been reached yet.

Among the low-phonon host crystals, fluorides are excellent candidates for rare-earth ion (RE^{3+}) doping leading to near-mid-infrared emissions. They exhibit better thermal properties and chemical stability as compared to their chloride and sulphide counterparts. They possess a low refractive index and good transparency. The RE^{3+} ions can be easily incorporated in fluoride crystals in high concentrations and they exhibit long excited-state lifetimes [10] and weak NR relaxation rates, while EM becomes significant at really high doping levels [11]. According to this argumentation, Tm^{3+} -doped fluoride crystals are attractive laser hosts for emission on the ${}^3\text{H}_4 \rightarrow {}^3\text{H}_5$ transition.

Indeed, so far, the main activity on bulk $\sim 2.3 \mu\text{m}$ Tm lasers focused on fluoride laser crystals and, in particular, $\text{Tm}:\text{LiYF}_4$ [12–15]. Pinto *et al.* reported on room-temperature continuous-wave (CW) $\text{Tm}:\text{LiYF}_4$ laser generating 0.22 W at $2.30 \mu\text{m}$ with a slope efficiency η of 15% and a continuous wavelength tuning in the range $2.20\text{--}2.46 \mu\text{m}$ [12]. Loiko *et al.* demonstrated power scaling of a similar laser up to 0.73 W with an increased $\eta = 34.6\%$ owing to energy-transfer upconversion (ETU), ${}^3\text{F}_4 + {}^3\text{F}_6 \rightarrow {}^3\text{H}_6 + {}^3\text{H}_4$, refilling the upper laser level [13]. Guillemot *et al.* recently showed the possibility of upconversion pumping of $\sim 2.3 \mu\text{m}$ $\text{Tm}:\text{LiYF}_4$ lasers [15].

Note that bulk $\sim 2.3 \mu\text{m}$ lasers based on low-phonon energy Tm^{3+} -doped glasses are also known [16].

Pulsed laser operation of $\text{Tm}:\text{LiYF}_4$ at $\sim 2.3 \mu\text{m}$ was also achieved [7,8,17,18]. Soulard *et al.* reported on SESAM mode-locked laser delivering 94 ps pulses at $\text{PRR} = 100 \text{ MHz}$ [7]. Canbaz *et al.* employed a $\text{Cr}^{2+}:\text{ZnSe}$ saturable absorber in a passively Q-switched laser however with moderate pulse characteristics, $1.2 \mu\text{s} / 13 \mu\text{J}$ (duration / energy) at a pulse repetition rate (PRR) of 2.1 kHz [17]. Later on, fs pulses were generated in a similar laser using Kerr-lens mode-locking and a graphene saturable absorber [8]. In the former case, the pulses were as short as 514 fs with an emission bandwidth of 15.4 nm at a PRR of 41.5 MHz.

Another fluoride crystal which seems very promising for mode-locked lasers around $2.3 \mu\text{m}$ is cubic potassium yttrium fluoride, KY_3F_{10} . It has a structure similar to that of CaF_2 (fluorite) while it offers a rare-earth substitutional site facilitating its doping [19]. KY_3F_{10} crystallizes in the $\text{KF} - \text{YF}_3$ binary system, it melts congruently at relatively low temperature allowing for Czochralski growth and it tolerates high RE^{3+} doping levels. However, KY_3F_{10} has been poorly studied for near-mid-infrared emissions of RE^{3+} ions. Regarding Tm^{3+} doping, the spectroscopic properties including Judd-Ofelt and crystal-field analysis and the first laser operation at $\sim 1.9 \mu\text{m}$ (at the ${}^3\text{F}_4 \rightarrow {}^3\text{H}_6$ transition) were reported [19,20]. Recently, thermo-optical properties and diode-pumped laser performance of a highly-doped crystal were studied. An 8 at.% $\text{Tm}:\text{KY}_3\text{F}_{10}$ laser generated 1.85 W at 1891 nm with $\eta = 26.1\%$ [21]. Braud *et al.* studied theoretically [22] and Muti *et al.* achieved laser operation on the ${}^3\text{H}_4 \rightarrow {}^3\text{H}_5$ transition yielding 0.12 W at 2343 nm with a low $\eta = 18\%$ [23]. Ho^{3+} -doped KY_3F_{10} crystals have also been employed for lasing at $\sim 2.1 \mu\text{m}$ [24].

Despite these results, the potential of $\text{Tm}:\text{KY}_3\text{F}_{10}$ to generate near-mid-infrared emissions has not been revealed so far. This may originate from the lack of key spectroscopic data, such as stimulated-emission cross-sections for the ${}^3\text{H}_4 \rightarrow {}^3\text{H}_5$ transition, the spectra of excited-state absorption or the rates of cross-relaxation governing the upper laser level lifetime. In the present work, we aimed to prove the unique ability of cubic $\text{Tm}:\text{KY}_3\text{F}_{10}$ crystal for highly-efficient and power-scalable operation at $\sim 2.3 \mu\text{m}$, based on a deep study of its spectroscopic features.

2. Crystal growth and spectroscopy

2.1. Crystal growth

The KY_3F_{10} compounds melts congruently at $\sim 1030 \text{ }^\circ\text{C}$. The $\text{Tm}:\text{KY}_3\text{F}_{10}$ crystal was grown by the Czochralski (Cz) method using an induction heating furnace. The growth charge was prepared from KF , YF_3 and TmF_3 powders (4N purity) taken in a stoichiometric ratio. They were well mixed and put into a glassy carbon crucible. The chamber was evacuated to 10^{-5} mbar

and the crucible was heated to 450 °C for 24 h to remove oxygen impurities. Then, the chamber was filled with high-purity Argon and CF₄ gases until atmospheric pressure and the crucible was heated up to the melting temperature for few hours. This helped to avoid formation of unwanted oxyfluoride phases. The crystal growth was carried out using an [100]-oriented seed of undoped KY₃F₁₀; the growth rate was 2–4 mm/h. After the growth, the crystal was removed from the melt and slowly cooled down to room-temperature (RT). The as-grown crystal was transparent and colorless. It was doped with 5.0 at.% Tm (in the crystal), resulting in a Tm³⁺ concentration $N_{\text{Tm}} = 7.63 \times 10^{20} \text{ cm}^{-3}$. The doping concentration was measured by inductively coupled plasma mass-spectrometry (ICP-MS).

Potassium triyttrium decafluoride (KY₃F₁₀) is a cubic (sp. gr. $Fm\bar{3}m - O^5_h$, No. 225) crystal. It represents an anion-excess $2 \times 2 \times 2$ superstructure of fluorite (CaF₂) [25]. KY₃F₁₀ is a representative of a series M_nX_{2n+2} (M = K, Y, X = F) for $n = 4$. In the structure of KY₃F₁₀, two ionic groups $[KY_3F_8]^{2+}$ and $[KY_3F_{12}]^{2-}$ alternate in the directions of three cubic axes [26]. It exhibits a single crystallographic site for Y³⁺ ions (local symmetry: C_{4v} , VIII-fold \tilde{F} coordination) [19]. The Tm³⁺ ions substitute to Y³⁺ in distorted square antiprisms $[Y|\text{TmF}_8]$. The crystal exhibits natural (111) cleavage planes.

For laser experiments, we cut a cylindrical sample (diameter: 6 mm, thickness t : 3.3 mm). Its input and output faces were polished to laser quality and remained uncoated.

2.2. Ground- and excited-state absorption

The scheme of energy-levels of Tm³⁺ ions in KY₃F₁₀ [19] is shown in Fig. 1. The bandgap of the host crystal E_g is $\sim 10 \text{ eV}$ [21]. All the spectroscopic studies were performed at RT (20 °C).

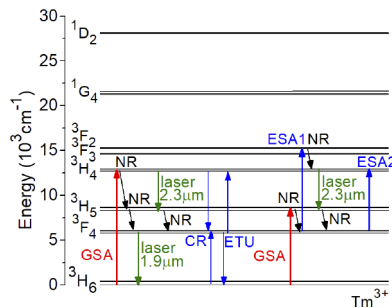


Fig. 1. The scheme of energy-levels of Tm³⁺ ions in cubic KY₃F₁₀ [19] showing the relevant spectroscopic processes: GSA and ESA – ground- and excited-state absorption, respectively, NR – non-radiative relaxation, CR – cross-relaxation, ETU – energy-transfer upconversion. Black and red arrows – pump and laser transitions, respectively.

The ground-state absorption (GSA) cross-sections, σ_{GSA} , were determined from absorption spectra measured using a spectrophotometer (Lambda 1050, Perkin Elmer) with a resolution of 0.1 nm. The GSA spectra for transitions $^3\text{H}_6 \rightarrow ^3\text{H}_4$, $^3\text{H}_5$ and $^3\text{H}_4$ are shown in Fig. 2. For the $^3\text{H}_6 \rightarrow ^3\text{H}_4$ transition (conventional pumping), the maximum σ_{GSA} is $6.6 \times 10^{-21} \text{ cm}^2$ at 778.4 nm and the full width at half maximum (FWHM) of the absorption peak is 3.8 nm.

The excited-state absorption (ESA) cross-sections, σ_{ESA} , were determined using a pump-probe technique [27]. A homemade color center laser tunable between 1.5–1.7 μm was used as pump source to excite Tm³⁺ ions at 1650 nm into the $^3\text{F}_4$ level. The pump power was 1 W. A tungsten-halogen lamp (Oriel, model 68830) was used to probe the absorption transitions from the $^3\text{F}_4$ excited state. The laser pump and the broadband light probe were modulated at a different frequencies (10 Hz and 1 kHz, respectively) and the transmitted probe beam was processed by a cascade of two lock-in amplifiers [28] enabling to record simultaneously the GSA and ESA

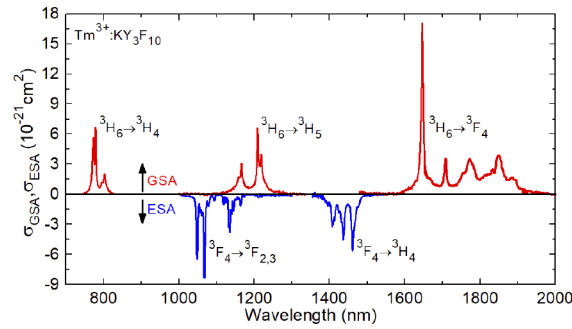


Fig. 2. Ground-state absorption (GSA) and excited-state absorption (ESA) cross-sections, σ_{GSA} and σ_{ESA} , respectively, for Tm^{3+} ions in KY_3F_{10} .

spectra. The GSA was used to calibrate the ESA spectra in cross-sections. The measurements were done in unpolarized light. The spectral resolution was 0.2 nm. A photomultiplier tube (Hamamatsu 5108) was used to detect the transmitted light at 0.8–1.2 μm and an InGaAs chip (Hamamatsu G5832) was implemented for the range of 1.2–1.6 μm .

The first studied ESA band (1.05–1.22 μm) is related to the ${}^3\text{F}_4 \rightarrow {}^3\text{F}_{2,3}$ transition and it spectrally overlaps with the GSA band ${}^3\text{H}_6 \rightarrow {}^3\text{H}_5$. The maximum $\sigma_{\text{ESA}} = 8.3 \times 10^{-21} \text{ cm}^2$ at 1067.5 nm (FWHM = 4.3 nm). There is another intense peak at slightly shorter wavelength (1048.1 nm) with $\sigma_{\text{ESA}} = 6.5 \times 10^{-21} \text{ cm}^2$ and FWHM = 4.8 nm selected for ESA-assisted pumping (Section 3.4). The corresponding GSA cross-section is below $0.01 \times 10^{-21} \text{ cm}^2$ corresponding to a phonon sideband.

The second studied ESA band (1.38–1.52 μm) is related to the ${}^3\text{F}_4 \rightarrow {}^3\text{H}_4$ transition and it overlaps with the ${}^3\text{H}_6 \rightarrow {}^3\text{F}_4$ absorption band. This ESA band is less intense, with a maximum σ_{ESA} of $5.5 \times 10^{-21} \text{ cm}^2$ at 1461.0 nm (FWHM = 9.6 nm), and its overlap with the GSA transition is less pronounced.

According to the Judd-Ofelt analysis of GSA transitions, the intensity parameters are $\Omega_2 = 1.907$, $\Omega_4 = 1.531$ and $\Omega_6 = 1.565$ [in 10^{-20} cm^2] [19].

2.3. Stimulated-emission

The stimulated-emission (SE) cross-sections, σ_{SE} , for the ${}^3\text{F}_4 \rightarrow {}^3\text{H}_6$ and ${}^3\text{H}_4 \rightarrow {}^3\text{H}_5$ transitions were calculated using the Füchtbauer-Ladenburg formula [29] from the measured luminescence spectra. The refractive index of KY_3F_{10} n is ~ 1.49 [30]. The radiative lifetimes of the excited-states τ_{rad} were determined using samples with low doping (0.1 at.% Tm) as $\tau_{\text{rad}}({}^3\text{F}_4) = 15.4 \text{ ms}$ and $\tau_{\text{rad}}({}^3\text{H}_4) = 1.9 \text{ ms}$ [20] and the luminescence branching ratio $B(\text{JJ}')$ for the ${}^3\text{H}_4 \rightarrow {}^3\text{H}_5$ transition was taken from the Judd-Ofelt analysis, $B(\text{JJ}') = 2.9\%$ [19].

The σ_{SE} spectra are shown in Fig. 3. For the ${}^3\text{F}_4 \rightarrow {}^3\text{H}_6$ transition, the maximum σ_{SE} equals $3.8 \times 10^{-21} \text{ cm}^2$ at 1845 nm. Compared to $\text{Tm}:\text{LiYF}_4$, the SE cross-sections are slightly lower and the emission band is blue-shifted. Thus, $\text{Tm}:\text{KY}_3\text{F}_{10}$ is not suitable for achieving fs pulses in mode-locked lasers operating on the ${}^3\text{F}_4 \rightarrow {}^3\text{H}_6$ transition as its emission is spectrally located well below 2 μm (overlapping with the structured water vapour absorption). Here and below, we use $\text{Tm}:\text{LiYF}_4$ as a reference material as it was mainly used for bulk $\sim 2.3 \mu\text{m}$ lasers.

For the ${}^3\text{H}_4 \rightarrow {}^3\text{H}_5$ transition, σ_{SE} reaches $3.4 \times 10^{-21} \text{ cm}^2$ at 2345 nm. The emission bandwidth $\Delta\lambda_{\text{em}}$ (FWHM) is 53.8 nm. Compared to $\text{Tm}:\text{LiYF}_4$ ($\Delta\lambda_{\text{em}} = 26.3 \text{ nm}$, centered at 2305 nm for π -polarization), $\text{Tm}:\text{KY}_3\text{F}_{10}$ provides much broader emission spectra on this transition whilst with lower SE cross-sections. Thus, it is attractive for ultrashort pulse generation at $\sim 2.3 \mu\text{m}$. Previously for $\text{Tm}:\text{KY}_3\text{F}_{10}$, σ_{SE} was estimated from the laser threshold as $8.1 \pm 0.3 \times 10^{-21} \text{ cm}^2$ [23] which is higher than the value determined in the present work.

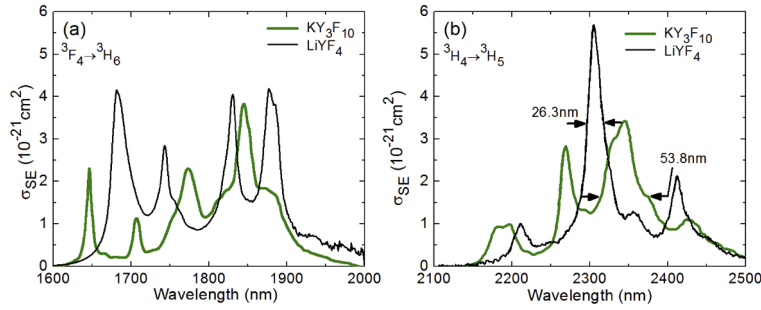


Fig. 3. Stimulated-emission (SE) cross-section, σ_{SE} , spectra for (a) ${}^3F_4 \rightarrow {}^3H_6$ and (b) ${}^3H_4 \rightarrow {}^3H_5$ transitions of Tm^{3+} ions in KY_3F_{10} . The spectra for $\text{Tm}:\text{LiYF}_4$ are given for comparison (for π -polarization). The values in (b) indicate emission bandwidth.

2.4. Luminescence decay

For luminescence decay studies, we used a nanosecond (ns) optical parametric oscillator (OPO, Horizon, Continuum) tuned to 778 nm as excitation source. The luminescence was detected using a 1/4 m monochromator (Oriel 77200), an InGaAs detector and a digital oscilloscope. To avoid radiation trapping, the pinhole method was used. The luminescence decay curves were measured at 1850 nm and 810 nm (luminescence from the 3F_4 and 3H_4 states, respectively).

The luminescence lifetime τ_{lum} of the 3F_4 state is 9.13 ms which is shorter than the value at low Tm^{3+} doping (15.4 ms) [20]. The luminescence decay curve, Fig. 4(a), is well fitted with a single-exponential law in agreement with a single Tm^{3+} incorporation site. For the 3H_4 state, τ_{lum} equals 24 μs , Fig. 4(b). It is notably quenched with respect to the intrinsic lifetime (in the limit of low doping), $\tau_0 = 1.9 \text{ ms}$ [20], due to the efficient CR process. This quenching is described as with $(1/\tau_{lum}) = (1/\tau_0) + W_{CR}$, where W_{CR} is the CR (self-quenching) rate, showing a quadratic dependence on the Tm^{3+} concentration, $W_{CR} = C_{CR} \cdot N_{\text{Tm}}^2$. By fitting the experimental points on $\tau_{lum}({}^3H_4)$ (from this work and [20,23]), Fig. 4(c), we estimated the concentration-independent CR parameter $C_{CR} = 0.28 \pm 0.1 \times 10^{-37} \text{ s}^{-1} \text{ cm}^6$, being similar to that of $\text{Tm}:\text{LiYF}_4$ [13].

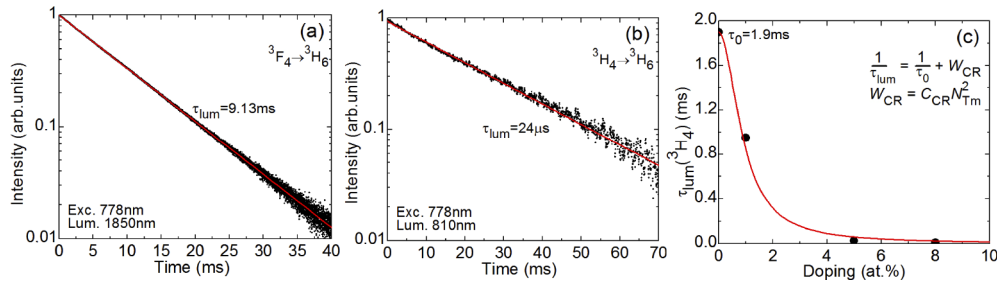


Fig. 4. Lifetime studies for Tm^{3+} ions in KY_3F_{10} : (a) luminescence decay from the 3F_4 state, $\lambda_{exc} = 778 \text{ nm}$, $\lambda_{lum} = 1850 \text{ nm}$. The measurement using the smallest pinhole (0.5 mm); (b) luminescence decay from the 3H_4 state, $\lambda_{exc} = 778 \text{ nm}$, $\lambda_{lum} = 810 \text{ nm}$; (c) luminescence lifetime τ_{lum} of the 3H_4 state vs. the doping concentration: circles – experimental data (this work and [20,23]), curve – their fit.

3. Laser operation

3.1. Laser set-up

The laser performance of $\text{Tm}:\text{KY}_3\text{F}_{10}$ at $\sim 2.3 \mu\text{m}$ was studied in a linear plano-concave cavity, Fig. 5, composed of a flat pump mirror (PM) coated for high reflection (HR, $R > 99.7\%$) at

1.85–2.35 μm and having a transmission T of 77.7% at 0.77 μm and 94.3% at 1.05 μm and a set of concave (radius of curvature (RoC): -100 mm) output couplers (OCs) having a transmission T_{OC} of 0.7%, 1.3% and 4.0% at the laser wavelength (2.34 μm). To suppress the unwanted ~ 1.9 μm emission (the ${}^3\text{F}_4 \rightarrow {}^3\text{H}_6$ transition), the OCs provided high transmission ($T > 90\%$) at this wavelength. The laser crystal was placed near the PM separated by ~ 1 mm at normal incidence. It was mounted on a passively-cooled Cu-holder using a silver paste to optimize heat removal. The geometrical cavity length L_{cav} was ~ 100 mm.

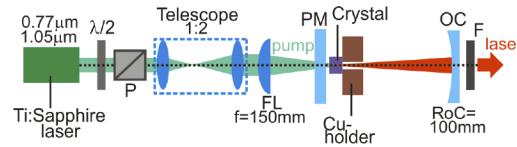


Fig. 5. Scheme of the Tm:KY₃F₁₀ laser: P – Glan-Taylor polarizer, $\lambda/2$ – rotatory half-wave plate, TL – telescope, FL – focusing lens, PM – pump mirror, OC – output coupler, F – band-pass filter.

As pump source, we used a Ti:Sapphire laser (3900S, Spectra Physics) delivering up to 3.9 W at 773 nm and 1.2 W at 1048 nm in the fundamental mode ($M^2 \approx 1$). The incident pump power was varied using a Glan-Taylor polarizer and a rotatable $\lambda/2$ plate. The pump beam was first expanded using a telescope containing two AR-coated spherical lenses (focal lengths: $f = 50$ mm and 100 mm) and then focused into the crystal through the PM using an achromatic CaF₂ lens ($f = 150$ mm). The measured pump spot radius at the focal point w_P was 60 ± 10 μm . Due to the reflectivity of the OCs at the pump wavelength ($R = 98\%$ at 0.77 μm and 20% at 1.05 μm), the pumping was in a double-pass. The thermal lens in Tm:KY₃F₁₀ is negative (its optical power $D = 1/f < 0$), determined by the so-called “generalized” thermo-optic coefficient $\chi = -4.1 \times 10^{-6}$ K⁻¹ at ~ 2 μm [21]. The radius of the fundamental laser mode in the crystal w_L was calculated using the ABCD method accounting for the thermal lens. As the thermal lens is pump-dependent, w_L is expected to decrease slowly with the pump power in the range 65–58 ± 5 μm . Here, we used the value of $L_{\text{cav}} = 99.9$ mm.

For the pump wavelength λ_P of 773 nm, the pump absorption was taken at the small-signal limit. For a single pass of the pump, $\eta_{\text{abs0}(1\text{-pass})} = (1 - R_F)[1 - \exp(-\sigma_{\text{GSA}} N_{\text{Tm}} t)] = 75.6\%$, where R_F is the Fresnel loss at the uncoated surface, so that for 2-passes we calculated $\eta_{\text{abs0}(2\text{-pass})} = 88.7\%$. This approach does not overestimate the slope efficiency which may be slightly higher due to the ground-state bleaching leading to decreased pump absorption. For $\lambda_P = 1048$ nm, the pump absorption was determined under lasing conditions by monitoring the residual (non-absorbed) pump after the OC. It increased gradually with the pump power reaching $\eta_{\text{abs,L}(2\text{-pass})} = 66.5 \pm 1\%$ above the laser threshold.

For comparison, we also studied the laser performance of Tm:KY₃F₁₀ at ~ 1.9 μm . For this, the same PM was used while the OCs (RoC = -100 mm) had a transmission $T_{\text{OC}} = 5\%$, 8% or 10% at the laser wavelength (~ 1.88 μm). Their reflectivity at the pump wavelength (0.77 μm) was $\sim 46\%$. The estimated pump absorption $\eta_{\text{abs0}(2\text{-pass})}$ was 80.2%.

The laser output was filtered from the residual pump using a band-pass filter (FB2250-500, Thorlabs). The laser emission spectra were measured with an optical spectrum analyzer (resolution: 0.1 nm, AQ6375B, Yokogawa). The profile of the laser beam was captured in the far-field using a pyroelectric camera (PY-III-HR-C-A, Ophir). The beam quality factors $M^2_{x,y}$ were measured using an ISO-standard method employing a CaF₂ lens ($f = 150$ mm) placed after the OC. The oscilloscope traces of laser output were captured using a fast InGaAs photodetector (UPD-5N-IR2-P) and an 8 GHz digital oscilloscope (DSA70804B, Tektronix). The spectra of visible emission were measured using a CCD-based spectrometer (HR2000+, Ocean Optics).

For both studied laser transitions, ${}^3F_4 \rightarrow {}^3H_6$ and ${}^3H_4 \rightarrow {}^3H_5$, the Tm:KY₃F₁₀ laser operated in CW regime, Fig. 6. In the former case, weak relaxation oscillations were observed, which are typical for Tm lasers based on fluoride crystals with long upper laser level (3F_4) lifetimes [31]. For the $\sim 2.3 \mu\text{m}$ laser, intensity instabilities in the ms time scale were observed being suppressed well above the laser threshold.

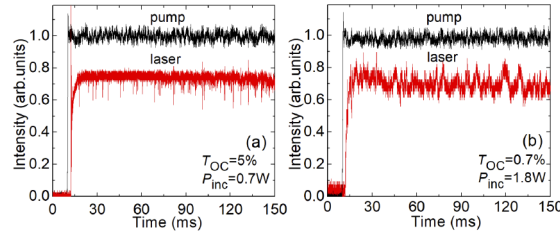


Fig. 6. Typical oscilloscope traces of incident pump and laser emission for the Tm:KY₃F₁₀ laser: operation at (a) ${}^3F_4 \rightarrow {}^3H_6$ and (b) ${}^3H_4 \rightarrow {}^3H_5$ transitions. $\lambda_P = 773 \text{ nm}$.

3.2. ${}^3F_4 \rightarrow {}^3H_6$ transition

First, we studied the laser operation at the ${}^3F_4 \rightarrow {}^3H_6$ transition ($\lambda_P = 773 \text{ nm}$). With conventional pumping, the laser scheme is as following. GSA of pump photons (${}^3H_6 \rightarrow {}^3H_4$) populates the pump level (3H_4). Then, there exist two options. First, the excited Tm³⁺ ion may relax down to the metastable state (upper laser level) 3H_4 by multiphonon NR relaxation via the short-living 3H_5 state (the most intense Raman vibration of KY₃F₁₀ has the energy $h\nu_{\text{ph}}$ of 378 cm^{-1} [21]). This process leads to one excitation in the 3F_4 state (part of the pump photon energy is lost as heat). Secondly, the excited Tm³⁺ ion may exchange its energy with another one in the ground-state via the CR process (${}^3H_4 + {}^3H_6 \rightarrow {}^3F_4 + {}^3F_4$) leading to 2 Tm³⁺ ions in the 3F_4 upper laser level and a reduced heat loading. The probability of the second process increases with Tm³⁺ doping.

The laser performance is summarized in Fig. 7. The Tm:KY₃F₁₀ laser generated a maximum output power of 1.38 W at 1884-1896nm with a slope efficiency $\eta = 59.4\%$ (vs. the incident pump power P_{inc} , fitting the output dependence well above the laser threshold, for $T_{\text{OC}} = 5\%$). The threshold pump power was as low as 60 mW and the optical-to-optical efficiency $\eta_{\text{opt}} = 58.7\%$ ($T_{\text{OC}} = 5\%$). No thermal roll-over was observed. The performance for other OCs ($T_{\text{OC}} = 8\%$ and 10%) was similar, the laser threshold increased to $\sim 130 \text{ mW}$.

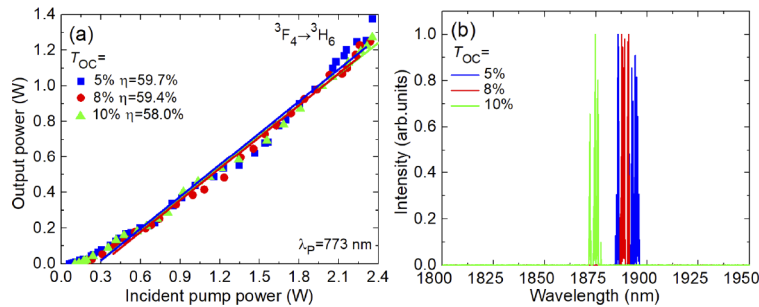


Fig. 7. Tm:KY₃F₁₀ laser operating at the ${}^3F_4 \rightarrow {}^3H_6$ transition: (a) input-output dependences, η – slope efficiency; (b) typical spectra of laser emission. The laser emission is unpolarized, $\lambda_P = 773 \text{ nm}$.

The laser emission was unpolarized (as cubic KY₃F₁₀ is optically isotropic). It appeared at $\sim 1.88 \mu\text{m}$ corresponding to the long-wavelength peak in the SE cross-section spectra, Fig.

3(a). Note that the ${}^3F_4 \rightarrow {}^3H_6$ Tm³⁺ laser transition exhibiting reabsorption corresponds to a quasi-three-level laser scheme. The multi-peak spectral behavior, Fig. 7(b), was due to etalon effects at the PM / crystal interfaces.

Accounting for $\eta_{\text{abs,L}(2\text{-pass})}$, the slope efficiency vs. the absorbed pump power was 74.4% (for $T_{\text{OC}} = 5\%$). This value is well above the Stokes limit, $\eta_{\text{St}} = \lambda_{\text{p}}/\lambda_{\text{L}} = 40.9\%$ (λ_{L} is the laser wavelength), confirming the efficacy of CR. According to the concentration-independent CR parameter, the CR rate $W_{\text{CR}} = 1.63 \times 10^4 \text{ s}^{-1}$ and the pump quantum efficiency $\eta_{\text{q1}} = 1.94 \pm 0.02$ (see [32] for the details about the calculation). Thus, assuming a roundtrip intracavity loss $2L = 0.5\%$, we calculated the upper limit for the laser slope efficiency, $\eta \leq \eta_{\text{St}} \cdot \eta_{\text{q1}} \cdot \eta_{\text{OC}} \cdot \eta_{\text{mode}} \approx 73\%$, where $\eta_{\text{OC}} = \ln[1 - T_{\text{OC}}]/\ln[1 - T_{\text{OC}} \cdot (1 - 2L)]$ is the output-coupling efficiency and $\eta_{\text{mode}} \approx 1$ is the mode overlap efficiency. This value is in good agreement with the experimental result.

The results from the present work on the $\sim 1.9 \mu\text{m}$ laser operation surpass those reported by Braud *et al.* with Ti:Sapphire pumping (0.27 W at 1846nm with $\eta = 42.5\%$ [20]) and by Chen *et al.* with diode-pumping (1.85 W at 1891nm with $\eta = 65.2\%$ [21], specified vs. the absorbed pump power in both cases), in terms of slope efficiency. Lower output power as compared to [21] is due to the limited available pump in our case.

3.3. ${}^3H_4 \rightarrow {}^3H_5$ transition: Conventional pumping

Furthermore, we studied the laser performance at the ${}^3H_4 \rightarrow {}^3H_5$ transition. With conventional pumping ($\lambda_{\text{p}} = 773 \text{ nm}$), the laser scheme is the following. After GSA (${}^3H_6 \rightarrow {}^3H_4$), the Tm³⁺ ions are excited to the upper laser level (3H_4). The lower laser level (3H_5) is fast depopulated by the NR relaxation thus avoiding the “bottleneck” effect like that observed in $\sim 2.8 \mu\text{m}$ Er lasers. However, the excitations are accumulated in the metastable state (3F_4) and may relax via the radiative or NR path (e.g., through energy-migration) towards the ground state. Thus, there is a certain fraction of the pump photon energy lost as heat. Moreover, CR is a detrimental effect for $\sim 2.3 \mu\text{m}$ lasers with conventional pumping. Indeed, CR depopulates the 3H_4 upper laser level and quenches its lifetime leading to an increased laser threshold.

The results on the input-output characteristics and the laser emission spectra are shown in Fig. 8. For $T_{\text{OC}} = 1.3\%$, the laser generated 0.84 W at 2331-2346 nm with $\eta = 47.7\%$. The laser threshold was at $P_{\text{inc}} = 0.93 \text{ W}$ and the maximum η_{opt} reached 27.5%. The input-output dependences were nonlinear near to the laser threshold. With an increase of the output coupling, the threshold notably increased (from 0.66 W for $T_{\text{OC}} = 0.7\%$ up to 1.64 W for $T_{\text{OC}} = 4\%$). The laser emission was unpolarized. Spectrally, it was centered at $\sim 2.34 \mu\text{m}$ for $T_{\text{OC}} > 1\%$ and for small output coupling (0.7%), additional lines at 2.270 μm and 2.319 μm were observed. This broadband emission behavior agrees well with the SE cross-section spectra, Fig. 3(b). It can be also understood considering the Stark splitting of the upper and lower laser manifolds, Fig. 8(c). Note that for the C_{4v} site symmetry, the number of sub-levels is 7 and 8 for $J = 4$ and 5, respectively [19]. The feature of KY_3F_{10} is that for majority of Tm³⁺ multiplets, the lower-lying Stark sub-levels are separated by a notable energy gap from a group of closely located higher-lying sub-levels. The emission wavelengths for transitions between sub-levels from the groups belonging to different multiplets are rather close and have a similar probability.

By tuning the pump source through the ${}^3H_6 \rightarrow {}^3H_4$ Tm³⁺ absorption band and measuring the laser output, we obtained the laser excitation spectrum, Fig. 9. The $\sim 2.3 \mu\text{m}$ laser operation was achieved for a broad range of λ_{p} , namely 760–811 nm. The optimum pump wavelength was at the second peak of the ${}^3H_6 \rightarrow {}^3H_4$ absorption band (773 nm). This is probably due to the double-pass pumping scheme.

The beam profile of the $\sim 2.3 \mu\text{m}$ laser was measured in the far-field, Fig. 10(a). The mode was nearly-circular with 1D intensity profiles well fitted with a Gaussian function. The beam quality factors M^2 along the horizontal (x) and vertical (y) directions were 2.1 ± 0.1 and 2.3 ± 0.1 , respectively. This is attributed to the action of negative thermal lens [21]. The increase of the

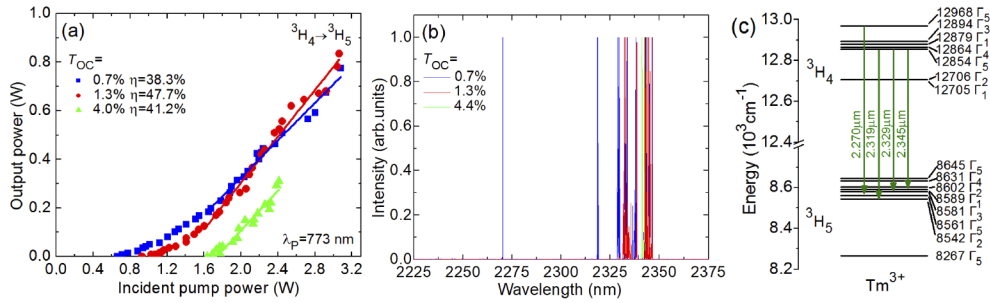


Fig. 8. Tm:KY₃F₁₀ laser operating at the ³H₄ → ³H₅ transition: (a) input-output dependences, η – slope efficiency; (b) typical laser emission spectra. The laser emission is unpolarized, $\lambda_p = 773$ nm; (c) details of the Stark splitting of the upper and lower laser levels showing the observed laser transitions (green arrows), Γ_i are the irreducible representations.

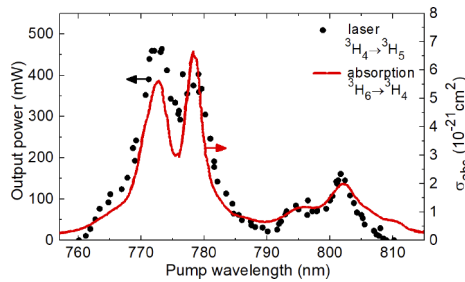


Fig. 9. Laser excitation curve for the Tm:KY₃F₁₀ laser: operation at the ³H₄ → ³H₅ transition by conventional pumping. Circles – output power of the laser ($T_{OC} = 0.7\%$), red curve – absorption cross-section spectrum for the ³H₆ → ³H₄ transition. The incident pump power is nearly constant over the studied range of pump wavelengths, $P_{inc} = 2.30 \pm 0.05$ W.

pump power leads to a size reduction of the laser mode (w_L) in the crystal, so that there is an increased probability for higher-order modes to be supported.

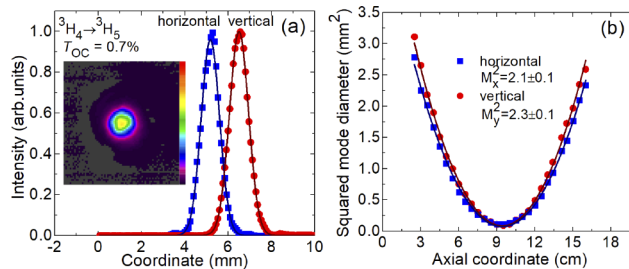


Fig. 10. Output laser beam of the Tm:KY₃F₁₀ laser operating at the ³H₄ → ³H₅ transition: (a) 1D intensity profiles along the horizontal and vertical directions (symbols) and their Gaussian fits (curves), inset – 2D mode profile, far-field; (b) evaluation of the beam quality factors $M^2_{x,y}$. $\lambda_p = 773$ nm, $P_{inc} = 1.7$ W, $T_{OC} = 0.7\%$.

Accounting for the pump absorption, the maximum η vs. P_{abs} reached 53.8% (for the output coupling of 1.3%). This value well exceeds the Stokes efficiency, $\eta_{St} = 33.0\%$. Let us discuss the physical nature of this behavior. Assuming only one energy-transfer process for Tm³⁺ ions, namely CR, the pump quantum efficiency for the ³H₄ → ³H₅ transition $\eta_{q2} < 1$ because CR

depopulates the upper laser level (3H_4). However, there is another energy-transfer process which compensates CR and refills the 3H_4 multiplet at the expense of the metastable state 3F_4 , i.e., ETU: $^3F_4 + ^3F_4 \rightarrow ^3H_6 + ^3H_4$. Accounting for both CR and ETU, η_{q2} can exceed unity.

Using the model of 2.3 μm Tm lasers described in [13], we calculated the η_{q2} values from the measured output power of the Tm:KY₃F₁₀ laser, Fig. 11. With the pump power, η_{q2} increases almost linearly and reaches beyond 1.5. For high $P_{\text{inc}} > 2.5$ W, a saturation of this dependence is observed ($\eta_{q2} \approx 1.6$ for $T_{\text{OC}} = 0.7\%$). This value agrees well with the determined laser slope efficiency vs. the absorbed pump power. η_{q2} increases with the pump power due to the fact that the CR effect is attenuated (due to ground-state bleaching) and ETU is magnified (due to the accumulation of ions in the 3F_4 level).

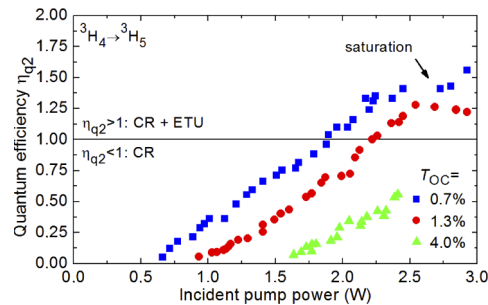


Fig. 11. Calculated pump quantum efficiency η_{q2} for the Tm:KY₃F₁₀ laser operating at the $^3H_4 \rightarrow ^3H_5$ transition ($\lambda_p = 773$ nm). Intracavity roundtrip losses: $2L = 0.7\%$.

3.4. $^3H_4 \rightarrow ^3H_5$ transition: Upconversion pumping

Another approach to pump the ~ 2.3 μm Tm lasers is the so-called upconversion (UC) pumping recently demonstrated [15]. In the present work, laser action is achieved for $\lambda_p = 1048$ nm. Its mechanism is the following. First, very few pump photons are absorbed by a non-resonant GSA transition ($^3H_6 \rightarrow ^3H_5$). The excitation to the 3H_5 multiplet is followed by an efficient NR relaxation down to the metastable 3F_4 state. Then, a resonant ESA1 process ($^3F_4 \rightarrow ^3F_{2,3}$) takes place again followed by NR relaxation ending in the upper laser level (3H_4). This process may become a photon avalanche [33] since the CR process refills the intermediate metastable state (3F_4) now acting as an efficient ground-state for the ~ 2.3 μm laser. In such a way, high absorption efficiencies can be reached despite a vanishing σ_{GSA} as shown in Fig. 2. Thus, for UC pumping, CR plays a positive role. Similarly to the case of conventional pumping, ETU has a positive effect as well.

The output performance of UC-pumped Tm:KY₃F₁₀ laser is shown in Fig. 12(a). The laser generated a maximum output power of 92 mW at 2270 & 2326-2344 nm with $\eta = 14.0\%$ and a laser threshold of 0.34 W. The laser slope efficiency vs. the absorbed pump power was 21.1%. Further power scaling was limited by the available pump. The broadband emission behavior was similar to the case of conventional pumping. UC pumping provides a similar slope efficiency (considering the same range of pump powers) and lower laser threshold as compared to conventional pumping. One can expect gradual increase of the slope efficiency for pump powers well exceeding the laser threshold, cf. Figure 8(a).

The laser excitation curve was also measured for UC pumping. Above 1052 nm, we were limited by the tuning range of the pump source (Ti:Sapphire laser). The results are shown in Fig. 12(b) together with the part of the cross-section spectra of GSA ($^3H_4 \rightarrow ^3H_5$) and ESA ($^3F_4 \rightarrow ^3F_{2,3}$) transitions spectrally overlapping with λ_p . The measured curve matches well with the

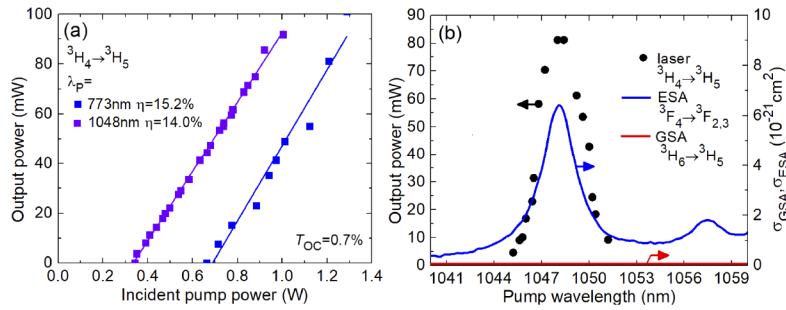


Fig. 12. Upconversion-pumped Tm:KY₃F₁₀ laser operating at the $^3\text{H}_4 \rightarrow ^3\text{H}_5$ transition: (a) input-output dependence, η – slope efficiency, $\lambda_p = 1048$ nm. The results for conventional pumping ($\lambda_p = 773$ nm) are given for comparison. $T_{OC} = 0.7\%$; (b) laser excitation curve: *circles* – output power of the laser ($P_{inc} = 0.92$ W, $T_{OC} = 0.7\%$), *blue and red curves* – parts of the ESA and GSA cross-section spectra for the $^3\text{F}_4 \rightarrow ^3\text{F}_{2,3}$ and $^3\text{H}_4 \rightarrow ^3\text{H}_5$ transitions, respectively.

ESA local peak at 1048.1 nm (note the almost zero and flat σ_{GSA} spectrum in the studied spectral range), confirming the key role of ESA in reaching population inversion.

In Table 1, we summarize the results on continuous-wave bulk thulium lasers operating at the $^3\text{H}_4 \rightarrow ^3\text{H}_5$ transition. Note that some previous studies focused on codoped crystals, e.g., with Yb³⁺, Tm³⁺ or Tm³⁺, Ho³⁺ ions [35,36], which is outside the scope of the present work. We report on the highest slope efficiency extracted from a ~ 2.3 μm Tm laser, and the highest output power achieved under Ti:Sapphire laser pumping. Watt-level output was generated recently by Wang *et al.* in a diode-pumped Tm:LiYF₄ laser [18].

Table 1. Output characteristics^a of continuous-wave ~ 2.3 μm thulium lasers reported so far

Crystal	Doping	Pump ^b	λ_p , nm	P_{th} , W	P_{out} , W	η , %	λ_L , μm	Ref.
Tm:LiYF ₄	1.5 at. %	TS	780	~ 0.1	0.22	15	~ 2.30	[12]
		TS	780	0.10	0.15	19	~ 2.31	[17]
	LD	785	1.2	1.15	19	2.306	[18]	
	3.5 at. %	TS	780	0.40	0.73	34.6	2.306	[13]
		TS	1040	0.20	0.10	14.6	2.302	[15]
Tm:KY ₃ F ₁₀	8 at. %	TS	778	0.34	0.12	18	2.343	[23]
	5 at. %	TS	773	0.93	0.84	47.7	2.331-2.346	This work
TS		1048	0.34	0.09	14.0	2.326-2.344	This work	
Tm:YAIO ₃	1.5 at. %	TS	776	0.44	0.25	17.8	2.273	[34]

^a λ_p – pump wavelength, P_{out} – output power, P_{th} – laser threshold, η – slope efficiency (both vs. the incident pump power), λ_L – laser wavelength.

^bTS – Ti:Sapphire laser, LD – laser diode.

4. Conclusions

To conclude, cubic Tm:KY₃F₁₀ crystals are promising for highly-efficient (slope efficiency $\sim 50\%$) and power-scalable (watt-level) near-mid-infrared lasers emitting at ~ 2.3 μm due to the $^3\text{H}_4 \rightarrow ^3\text{H}_5$ Tm³⁺ transition. This is because of (i) good thermal and thermo-optical properties allowing for power-scaling, (ii) long lifetimes of the excited-states and low-phonon nature of the host matrix minimizing the NR path, (iii) efficient ETU at moderate Tm³⁺ doping levels enhancing

the pump quantum efficiency for the ${}^3\text{H}_4 \rightarrow {}^3\text{H}_5$ transition up to 2, (iv) intense ESA facilitating upconversion pumping. We report on the record slope efficiency for any $\sim 2.3\ \mu\text{m}$ Tm laser (cf. Table 1) being comparable with that for the well-known ${}^3\text{F}_4 \rightarrow {}^3\text{H}_6$ laser transition [Fig. 7(a)], using a Tm:KY₃F₁₀ crystal.

Further power scaling in CW regime is expected when applying other pump sources, e.g., AlGaAs laser diodes emitting at $\sim 0.8\ \mu\text{m}$ (for conventional pumping) or Yb fiber lasers emitting at $\sim 1.05\text{--}1.07\ \mu\text{m}$ (for UC pumping), both being commercially available. In this way, multi-watt output is expected from $\sim 2.3\ \mu\text{m}$ Tm:KY₃F₁₀ lasers. In particular for UC pumping, further work is required to determine the upper limit for the slope efficiency. In the present work, this approach leads to η of only 21.1% (compare with $\eta = 53.8\%$ for conventional pumping, both vs. the absorbed pump power). However, this difference may originate from the different level of pump intensity above the laser threshold. Moreover, for UC pumping, more intense ESA peak at 1067.5 nm can be used. Further work on CW power scaling should also focus on the thermal lens measurements under $\sim 2.3\ \mu\text{m}$ lasing conditions.

The Tm:KY₃F₁₀ crystals are also promising for pulsed lasers. The relatively long upper laser level (${}^3\text{H}_4$) lifetime (for doping levels $< 5\ \text{at.}\%$ Tm) is favorable for passive Q-switching, e.g., with Cr²⁺:ZnSe crystals. The broadband emission properties at $\sim 2.34\ \mu\text{m}$ (emission bandwidth $> 50\ \text{nm}$) are also rather attractive for femtosecond mode-locked oscillators.

Funding

Agence Nationale de la Recherche (ANR-10-LABX-09-01), (ANR-19-CE08-0028).

Acknowledgments

This work was supported by French Agence Nationale de la Recherche (ANR) through the LabEx EMC3 (ANR-10-LABX-09-01), SPLENDID2 (ANR-19-CE08-0028), and the European project "NOVAMAT" co-funded by the European Community funds FEDER and the Normandie region.

Disclosures

The authors declare no conflicts of interest.

References

1. A. Schliesser, N. Picqué, and T. W. Hänsch, "Mid-infrared frequency combs," *Nat. Photonics* **6**(7), 440–449 (2012).
2. V. Petrov, "Frequency down-conversion of solid-state laser sources to the mid-infrared spectral range using non-oxide nonlinear crystals," *Prog. Quantum Electron.* **42**, 1–106 (2015).
3. A. Garnache, A. Liu, L. Cerutti, and A. Campargue, "Intracavity laser absorption spectroscopy with a vertical external cavity surface emitting laser at 2.3 μm : Application to water and carbon dioxide," *Chem. Phys. Lett.* **416**(1-3), 22–27 (2005).
4. S. T. Fard, W. Hofmann, P. T. Fard, G. Bohm, M. Ortsiefer, E. Kwok, M. C. Amann, and L. Chrostowski, "Optical absorption glucose measurements using 2.3 μm vertical-cavity semiconductor lasers," *IEEE Photonics Technol. Lett.* **20**(11), 930–932 (2008).
5. N. Tolstik, E. Sorokin, and I. T. Sorokina, "Graphene mode-locked Cr:ZnS laser with 41 fs pulse duration," *Opt. Express* **22**(5), 5564–5571 (2014).
6. T. J. Carrig, G. J. Wagner, A. Sennaroglu, J. Y. Jeong, and C. R. Pollock, "Mode-locked Cr²⁺:ZnSe laser," *Opt. Lett.* **25**(3), 168–170 (2000).
7. R. Souillard, A. Tyazhev, J. L. Doualan, A. Braud, A. Hideur, M. Laroche, B. Xu, and P. Camy, "2.3 μm Tm³⁺:YLF mode-locked laser," *Opt. Lett.* **42**(18), 3534–3536 (2017).
8. F. Canbaz, I. Yorulmaz, and A. Sennaroglu, "Kerr-lens mode-locked 2.3- μm Tm³⁺:YLF laser as a source of femtosecond pulses in the mid-infrared," *Opt. Lett.* **42**(19), 3964–3967 (2017).
9. J. Caird, L. DeShazer, and J. Nella, "Characteristics of room-temperature 2.3- μm laser emission from Tm³⁺ in YAG and YAlO₃," *IEEE J. Quantum Electron.* **11**(11), 874–881 (1975).
10. B. M. Walsh, N. P. Barnes, and B. Di Bartolo, "Branching ratios, cross sections, and radiative lifetimes of rare earth ions in solids: application to Tm³⁺ and Ho³⁺ ions in LiYF₄," *J. Appl. Phys.* **83**(5), 2772–2787 (1998).

11. R. Soulard, M. Salhi, G. Brasse, P. Loiko, J.-L. Doualan, L. Guillemot, A. Braud, A. Tyazhev, A. Hideur, and P. Camy, "Laser operation of highly-doped Tm:LiYF₄ epitaxies: towards thin-disk lasers," *Opt. Express* **27**(6), 9287–9301 (2019).
12. J. F. Pinto, L. Esterowitz, and G. H. Rosenblatt, "Tm³⁺:YLF laser continuously tunable between 2.20 and 2.46 μm," *Opt. Lett.* **19**(12), 883–885 (1994).
13. P. Loiko, R. Soulard, L. Guillemot, G. Brasse, J.-L. Doualan, A. Braud, A. Tyazhev, A. Hideur, B. Guichardaz, F. Druon, and P. Camy, "Efficient Tm:LiYF₄ lasers at ~2.3 μm: Effect of energy-transfer upconversion," *IEEE J. Quantum Electron.* **55**(6), 1–12 (2019).
14. I. Yorulmaz and A. Sennaroglu, "Low-threshold diode-pumped 2.3-μm Tm³⁺:YLF lasers," *IEEE J. Sel. Top. Quantum Electron.* **24**(5), 1–7 (2018).
15. L. Guillemot, P. Loiko, R. Soulard, A. Braud, J.-L. Doualan, A. Hideur, R. Moncorgé, and P. Camy, "Thulium laser at ~2.3 μm based on upconversion pumping," *Opt. Lett.* **44**(16), 4071–4074 (2019).
16. B. I. Denker, V. V. Dorofeev, B. I. Galagan, V. V. Koltashev, S. E. Motorin, S. E. Sverchkov, and V. G. Plotnichenko, "Rare-earth ions doped zinc-tellurite glass for 2÷3 μm lasers," *Appl. Phys. B* **124**(12), 235 (2018).
17. F. Canbaz, I. Yorulmaz, and A. Sennaroglu, "2.3-μm Tm³⁺:YLF laser passively Q-switched with a Cr²⁺:ZnSe saturable absorber," *Opt. Lett.* **42**(9), 1656–1659 (2017).
18. S. Wang, H. Huang, H. Chen, X. Liu, S. Liu, J. Xu, and D. Shen, "High efficiency nanosecond passively Q-switched 2.3 μm Tm:YLF laser using a ReSe₂-based saturable output coupler," *OSA Continuum* **2**(5), 1676–1682 (2019).
19. M. Diaf, A. Braud, C. Labbé J, L. Doualan, S. Girard, J. Margerie, R. Moncorgé, and M. Thuau, "Synthesis and spectroscopic studies of Tm³⁺-doped KY₃F₁₀ single crystals," *Can. J. Phys.* **77**(9), 693–697 (2000).
20. A. Braud, P. Tigreat, J. Doualan, and R. Moncorgé, "Spectroscopy and cw operation of a 1.85 μm Tm:KY₃F₁₀ laser," *Appl. Phys. B* **72**(8), 909–912 (2001).
21. M. Chen, P. Loiko, J. M. Serres, S. Veronesi, M. Tonelli, M. Aguiló, F. Díaz, J. E. Bae, T. G. Park, F. Rotermund, S. Dai, Z. Chen, U. Griebner, V. Petrov, and X. Mateos, "Fluorite-type Tm³⁺:KY₃F₁₀: A promising crystal for watt-level lasers at ~1.9 μm," *J. Alloys Compd.* **813**, 152176 (2020).
22. A. Braud, S. Girard, J. L. Doualan, M. Thuau, R. Moncorgé, and A. M. Tkachuk, "Energy-transfer processes in Yb:Tm-doped KY₃F₁₀, LiYF₄, and BaY₂F₈ single crystals for laser operation at 1.5 and 2.3 μm," *Phys. Rev. B* **61**(8), 5280–5292 (2000).
23. A. Muti, M. Tonelli, V. Petrov, and A. Sennaroglu, "Continuous-wave mid-infrared laser operation of Tm³⁺:KY₃F₁₀ at 2.3 μm," *Opt. Lett.* **44**(13), 3242–3245 (2019).
24. M. Schellhorn, D. Parisi, S. Veronesi, G. Bolognesi, M. Eichhorn, and M. Tonelli, "In-band pumped Ho³⁺:KY₃F₁₀ 2 μm laser," *Opt. Lett.* **38**(4), 504–506 (2013).
25. K. Friese, H. Krüger, V. Kahlenberg, T. Balić-Zunić, H. Emerich, J. Y. Gesland, and A. Grzechnik, "Study of the temperature dependence of the structure of KY₃F₁₀," *J. Phys.: Condens. Matter* **18**(9), 2677–2687 (2006).
26. A. Grzechnik, J. Nuss, K. Friese, J. Y. Gesland, and M. Jansen, "Refinement of the crystal structure of potassium triyttrium decafluoride, KY₃F₁₀," *Z. Kristallogr. - New Cryst. Struct.* **217**(1), 460 (2002).
27. S. Kück, L. Fornasiero, E. Mix, and G. Huber, "Excited state absorption and stimulated emission of Nd³⁺ in crystals. Part I: Y₃Al₅O₁₂, YAlO₃, and Y₂O₃," *Appl. Phys. B* **67**(2), 151–156 (1998).
28. P. Le Boulanger, J. L. Doualan, S. Girard, J. Margerie, and R. Moncorgé, "Excited-state absorption spectroscopy of Er³⁺-doped Y₃Al₅O₁₂, YVO₄, and phosphate glass," *Phys. Rev. B* **60**(16), 11380–11390 (1999).
29. B. Aull and H. Jenssen, "Vibronic interactions in Nd:YAG resulting in nonreciprocity of absorption and stimulated emission cross sections," *IEEE J. Quantum Electron.* **18**(5), 925–930 (1982).
30. P. Porcher and P. Caro, "Crystal field parameters for Eu³⁺ in KY₃F₁₀. III. Radiative and nonradiative transition probabilities," *J. Chem. Phys.* **68**(9), 4183–4187 (1978).
31. M. Schellhorn, S. Ngcobo, and C. Bollig, "High-power diode-pumped Tm:YLF slab laser," *Appl. Phys. B* **94**(2), 195–198 (2009).
32. E. C. Honea, R. J. Beach, S. B. Sutton, J. A. Speth, S. C. Mitchell, J. A. Skidmore, M. A. Emanuel, and S. A. Payne, "115-W Tm:YAG diode-pumped solid-state laser," *IEEE J. Quantum Electron.* **33**(9), 1592–1600 (1997).
33. M. F. Joubert, S. Guy, and B. Jacquier, "Model of the photon-avalanche effect," *Phys. Rev. B* **48**(14), 10031–10037 (1993).
34. L. Guillemot, P. Loiko, A. Braud, J.-L. Doualan, A. Hideur, M. Koselja, R. Moncorgé, and P. Camy, "Continuous-wave Tm:YAlO₃ laser at ~2.3 μm," *Opt. Lett.* **44**(20), 5077–5080 (2019).
35. A. Diening, P. A. Möbert, and G. Huber, "Diode-pumped continuous-wave, quasi-continuous-wave, and Q-switched laser operation of Yb³⁺, Tm³⁺:YLiF₄ at 1.5 and 2.3 μm," *J. Appl. Phys.* **84**(11), 5900–5904 (1998).
36. G. Kintz, L. Esterowitz, and R. Allen, "Cascade laser emission at 2.31 and 2.08 μm from laser diode pumped Tm,Ho:LiYF₄ at room temperature," in *Advanced Solid State Lasers* (Optical Society of America, 1987), paper MC2.